Available online at www.sciencedirect.com

ScienceDirect

Procedia Structural Integrity 8 (2018) 92–101

Structural Integrity Procedia

www.elsevier.com/locate/procedia

AIAS 2017 International Conference on Stress Analysis, AIAS 2017, 6-9 September 2017, Pisa, Italy

Vibration fatigue tests by tri-axis shaker: design of an innovative system for uncoupled bending/torsion loading

Davide Zanellati[a]*, Denis Benasciutti[a], Roberto Tovo[a]

[a]*Department of Engineering, University of Ferrara, via Saragat 1, 44122, Ferrara, Italy*

Abstract

An innovative system for bending-torsion fatigue tests by tri-axis shaker is designed and presented. The system mounts a cylindrical specimen with eccentric tip mass, excited by horizontal and vertical base accelerations. A lateral thin plate prevents specimen horizontal displacement and allows torsional and bending deformations to be controlled independently. A lumped-mass model is first used to verify if input accelerations and resultant dynamic forces, required in testing, comply with shaker specifications. A finite element model is then used to perform both modal and harmonic analyses, necessary to determine the system natural frequencies and the dynamic response under horizontal and vertical accelerations. Experimental measures on a prototype are finally used to gather preliminary information for validating the numerical model and to verify that the proposed testing system can control bending and torsion loadings independently.

Peer-review under responsibility of the Scientific Committee of AIAS 2017 International Conference on Stress Analysis

Keywords: tri-axis shaker; vibration testing; uncoupled bending/torsion loading; multiaxial fatigue; system design

1. Introduction

Multiaxial random fatigue loadings are very common in vibrating structures and components. Fatigue life can profitably be estimated by spectral methods defined in frequency domain (Benasciutti and Tovo (2005), (2006)). Over the last decades, a number of methods has been proposed to analyze Gaussian and non-Gaussian stationary uniaxial and multi-axial random loadings, with narrow-band or wide-band frequency content (Benasciutti and Tovo

* Corresponding author. Tel.: +39-0532-974104; fax: +39-0532-974870.
E-mail address: davide.zanellati@unife.it

Peer-review under responsibility of the Scientific Committee of AIAS 2017 International Conference on Stress Analysis
10.1016/j.prostr.2017.12.011

(2005), (2006), (2016)). Despite great improvements in theoretical and numerical investigations, experimental laboratory tests still remain an important step to check the accuracy of spectral methods against experimental data, as well as to perform full-scale durability tests that resemble actual service conditions very closely.

Laboratory tests with multiaxial random loading generally apply an imposed force or displacement (e.g. by a servo-hydraulic machine), or a base acceleration by a shaker (thus allowing for higher testing frequencies). Various testing methodologies that differ by testing machines, specimen geometry and type of excitation have been proposed in the literature. Servo-hydraulic machines usually adopt cylindrical specimens, whereas shakers range from simple (plate, cylindrical) to more elaborated specimens (Y-geometry), which are usually fixed to the shaker table and excited by a base acceleration.

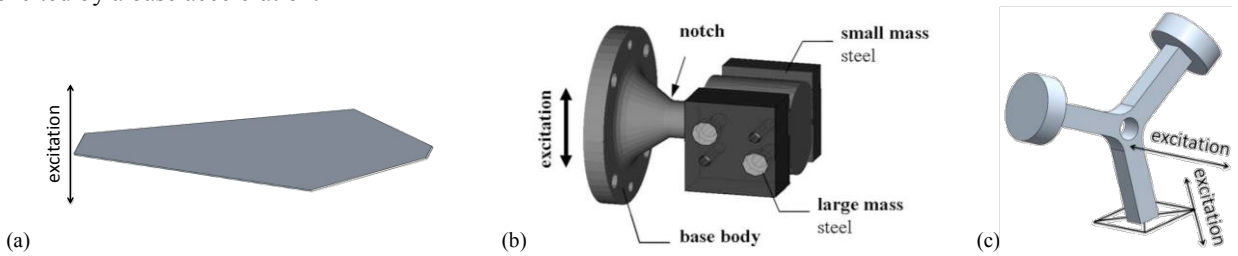

Fig. 1. (a) trapezoidal plate specimen; (b) cylindrical specimen with eccentric tip mass; (c) Y-specimen

Plate specimen with square or rectangular shape (often with lateral notches), excited at resonance by base vertical acceleration, represent the simplest and cheapest layout to realize a bending loading (uniaxial stress) (Ghielmetti et al. (2011), Khalij et al. (2015), Ellyson et al. (2017)). A "trapezoidal" plate specimen (Fig. 1a) was used, instead, for in-phase biaxial bending (with stress ratio $\sigma_y/\sigma_x \cong 0.59$) to simulate turbine blades response at resonance (George et al. (2004)). The stress ratio depends on the specimen geometry and cannot be changed. A biaxial normal stress was also obtained by a thin cruciform specimen used in (Łagoda et al. (2000)). With plate specimens, obtaining a torsion loading is yet not possible.

Cylindrical specimens (smooth, notched or with transverse holes) were adopted in different studies (Łagoda et al. (2005), Niesłony et al. (2012), Kim et al. (2011)). The layout in Kim et al. (2011) allows for simple bending when the specimen mounted on a shaker is excited by a base vertical acceleration. Two shakers controlled independently are used in Łagoda et al. (2005) to apply bending, torsion or both (with any correlation), their relative intensities being controlled by the amount of load eccentricity with respect to the specimen axis. Instead, in Niesłony et al. (2012), a servo-hydraulic multiaxial testing machine was used to apply bending-torsion loading.

An interesting layout for bending-torsion loading by shaker was proposed in Nguyen et al. (2011): a cantilever cylindrical specimen with two tip masses, and resonating under a base vertical (uniaxial) acceleration. The free specimen extremity mounts two unequal masses (i.e. an eccentric net mass), whose barycenter is not aligned with the specimen axis (Fig. 1b). This eccentricity then allows for torsion loading, even when the specimen is excited by uniaxial vertical acceleration. The intensity of bending loading is controlled by the mass value, the intensity of torsion loading by the eccentricity value (zero eccentricity would give simple bending, with no torsion). The only restriction is that torsion is always coupled with bending, i.e. it is not possible to have only torsion without bending.

A certainly more elaborated, yet less cheap, testing layout is the Y-specimen designed in Česnik et al. (2012). The specimen has a central hole and two tip masses and it develops a multiaxial stress when subjected to horizontal and vertical base excitation. The relative amount of shear-to-normal stress ratio is, however, predetermined by the specimen geometry and cannot be changed arbitrarily.

Among all those surveyed above, the layout proposed by Nguyen et al. (2011) sounds very promising, as it allows for bending-torsion random loading by vertical acceleration imposed by a uniaxial shaker. The only limitation is that torsion cannot be uncoupled from bending. The aim of the present paper is to design a testing system that, when excited by a tri-axis shaker, induces a fully uncoupled bending and torsion loading. The system can apply either bending or torsion, or both with any prescribed phase shift. Starting from the layout in Fig. 1b, the idea is to introduce a thin plate at the specimen free extremity to prevent the bending deformation when the specimen is loaded in torsion (see Fig. 2).

2. Innovative testing system

A preliminary system layout was developed in Zanellati et al. (2016), see Fig. 2a. The system is composed of a specimen with smooth notch. A cantilever beam with two tip masses is mounted at the specimen free extremity. Both the cantilever beam and the specimen extremity are clamped to the base by a thin plate, which prevents any vertical displacement. Being very thin, the plate is very flexible in bending and thus it does not impede the torsional rotation of the specimen. Therefore, a vertical excitation causes only a torsional loading induced by tip masses, whereas vertical bending is impeded by the thin plate. A horizontal excitation, instead, induces only a bending loading on the horizontal plane.

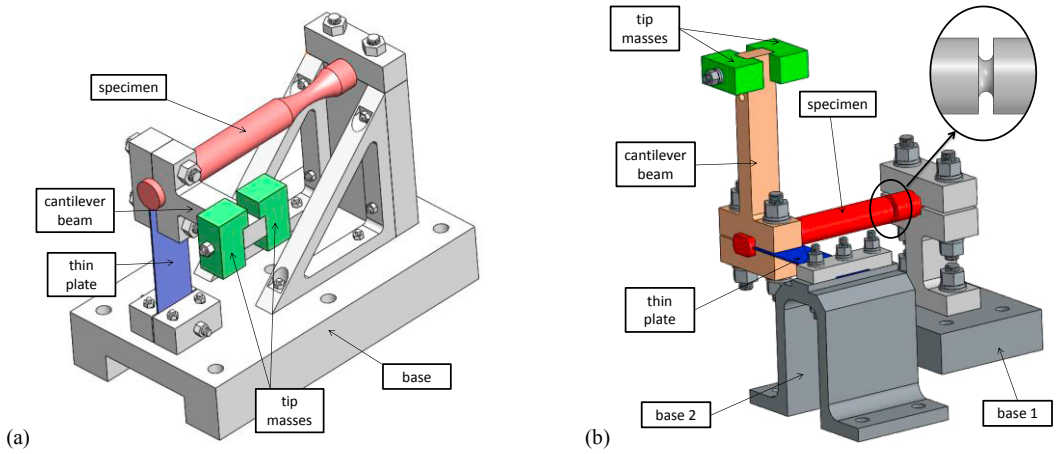

Fig. 2. Proposed testing system: (a) preliminary layout; (b) improved layout.

A preliminary modal analysis (Zanellati et al. (2016)) showed that this layout was very promising, because its bending and torsion resonance frequencies were well separated and so easy to be excited individually. However, the dynamic forces required to produce specimen failure by shaker vibration were too large and so a new configuration was designed (Fig. 2b).

As action plan to reduce the dynamic forces, by decreasing both masses and accelerations, different options were embraced: revising the system layout and also considering lighter materials to reduce the overall system weight, increasing the cantilever beam length and using a notched specimen to decrease input accelerations.

The new layout, obtained by a 90° clockwise rotation from its predecessor, retains the same working principle. Indeed, also here a thin plate clamps the specimen extremity to the base, preventing the horizontal displacement, while permitting the torsion induced by the eccentric tip masses. Compared to the first configuration, a horizontal excitation induces only torsional loading, while a vertical excitation induces only bending loading. Moreover, the diameter of net cross-sectional area is decreased from 10 to 8 mm, while the length of cantilever beam is increased from 60 to 120 mm. Moreover, the two clamps at both specimen ends (base 1 and base 2 in Fig. 2b) are completely reviewed and have been planned in 6082 aluminum alloy instead of S235JR steel. The specimen now has a U-notch with a tip radius of 2 mm, whose stress concentration factors are $K_{t,b}$=1.58 for bending and $K_{t,t}$=1.35 for torsion (Pilkey et al. (2008)). The overall weight m_{system} of the new system is decreased from 10.83 to 4.65 kg.

3. Analytical model

As a preliminary analysis, a lumped-mass analytical model (Fig. 3) was adopted to approximate the system response under quasi-static condition (e.g. low vibrating frequency) and to get a first estimate of input accelerations required for bending and torsion loading in experimental tests on shaker.

In the model, the specimen, the eccentric masses and the cantilever beam are represented by concentrated masses placed in their barycenter. Being very thin, the plate mass is neglected into the model. In addition, the plate should

not impede the vertical bending and the torsional rotation of the specimen, while it prevents the horizontal bending of the specimen.

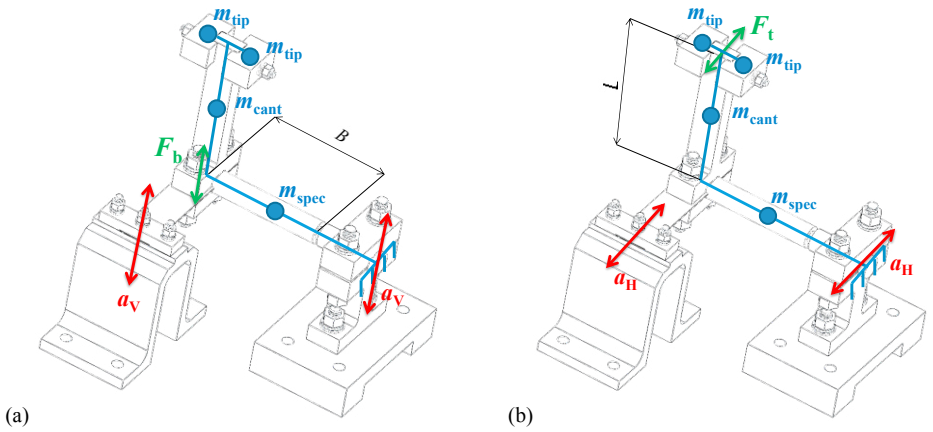

Fig. 3. Lumped-mass model and dynamic forces for: (a) bending; (b) torsion.

Under quasi-static condition, in first approximation, the formula $F=m\cdot a$ is valid, where a is the input acceleration given by shaker and m is the concentrated mass in the model.

To obtain a bending loading, a vertical acceleration a_V is applied, which gives the following force $F_b=F_{tip}+F_{spec}$, where $F_{tip}=(2m_{tip}+m_{cant})\cdot a_V$ acts on the specimen extremity and $F_{spec}=m_{spec}\cdot a_V$ acts on specimen barycenter. The eccentric tip mass is m_{tip}, the cantilever mass is m_{cant} and the specimen mass is m_{spec}. The resultant bending moment at the notch is $M_b=F_{tip}\cdot B+F_{spec}\cdot B/2$, where B is the distance between the specimen extremity and the notch. Thus, the maximum bending stress on the notch is $\sigma_{p,notch}=(M_b/W_b)\cdot K_{t,b}$, where W_b is the elastic bending section modulus.

Similarly, to obtain a torsion loading, a horizontal acceleration a_H is applied, which gives the force $F_t=F_{mass}+F_{cant}$, where $F_{mass}=2m_{tip}\cdot a_H$ acts on the cantilever extremity and $F_{cant}=m_{cant}\cdot a_H$ acts on cantilever barycenter. Under a horizontal acceleration, the plate impedes the movement of the specimen mass m_{spec}, which in fact is not included into the force F_t. The resultant torsional moment at the notch is $M_t=F_{mass}\cdot L+F_{cant}\cdot L/2$, where L is the distance between the tip masses and the longitudinal axis of specimen. The maximum shear stress on the notch is $\tau_{p,notch}=(M_t/W_t)\cdot K_{t,t}$, where W_t is the elastic torsional section modulus.

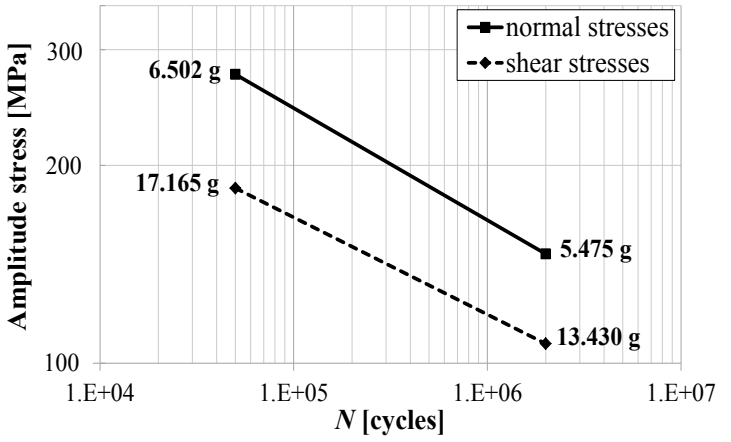

Fig. 4. S-N curve for notched specimen for normal (solid line) and shear stresses (dashed line).

Since the purpose of this research falls within the field of high-cycle fatigue, the acceleration values a_V, a_H leading to specimen failure at $5 \cdot 10^4$ and at $2 \cdot 10^6$ cycles (as lower and upper limits of life fatigue) are considered. For both bending and torsion models, such accelerations are obtained (see Eq. (1)) by inverting the previous expressions and by equating the notch stress $\sigma_{p,notch}$ and $\tau_{p,notch}$ to the fatigue strength at the previous cycle numbers.

$$a_V = \frac{\sigma_{p,notch} \cdot W_b}{(2m_{tip} + m_{cant} + 0.5m_{spec}) \cdot B \cdot K_{t,b}} \qquad a_H = \frac{\tau_{p,notch} \cdot W_t}{(2m_{tip} + 0.5m_{cant}) \cdot L \cdot K_{t,t}} \tag{1}$$

Considering the steel S355JR as specimen material, the fatigue amplitude strength for plain material at $2 \cdot 10^6$ cycles is, respectively, $\sigma_{A0,-1}$=231.7 MPa for normal stress and $\tau_{A0,-1}$=144.5 MPa for shear stress, and the inverse slopes of S-N curves are, respectively, k_σ=21.21 and k_τ=15.04 (Benasciutti (2014)). For the notched specimen, the fatigue strength is scaled as $\sigma_{An,-1}=\sigma_{A0,-1}/K_{t,b}$ and $\tau_{An,-1}= \tau_{A0,-1}/K_{t,t}$ (Schijve (2009)), while the inverse slopes are $k_{\sigma,n}$=5.84 and $k_{\tau,n}$=6.75.

The S-N curves for the notch specimen allow the highest accelerations at $5 \cdot 10^4$ cycles to be determined. For example, a horizontal acceleration of 17.165 g is required to have specimen failure under torsion at $5 \cdot 10^4$ cycles. Knowing that the weight system is m_{system}=4.65 kg, the corresponding force is 0.78 kN, which is much lower than the limit force F_{shaker}=10 kN allowable by the tri-axis shaker available in our laboratory. The other accelerations and corresponding forces are smaller (see Fig. 4). Therefore, the results estimated by the analytical model emphasize how the designed layout requires input accelerations which are perfectly compatible with shaker technical feature. These estimates will be compared to finite element harmonic analysis in Section 5.

4. Finite element model

A finite element model was then used to simulate more realistically the system dynamic behavior under horizontal and vertical accelerations. The results will be employed to prove that, as stated above, also the new system allows fully uncoupled bending-torsion and to calculate the input accelerations required in experimental tests more accurately.

The hypothesis of linear, elastic and isotropic material is assumed. The density, Young's modulus and Poisson's ratio are 8027 kg/m3, 200 GPa and 0.3, respectively, typical values of S355JR steel.

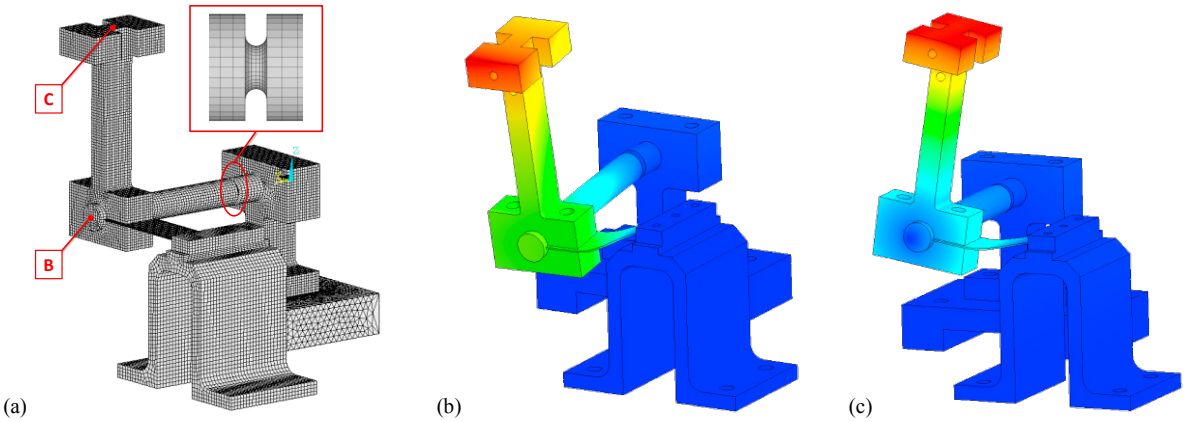

Fig. 5. (a) Finite element model; (b) modal shape in bending; (c) modal shape in torsion.

A structured mesh was used everywhere, except on base 1 because of its complex geometry (Fig.5a). The average element size in the notch is lower than 0.5 mm, instead it is 1 mm elsewhere. A 8-node solid finite element, with three degrees of freedom for each node, was adopted. The nodes lying on the bottom surfaces of the clamps (base 1 and base 2 in Fig. 2b) were fully constrained.

A modal analysis was performed to identify the first two resonance frequencies: the first at 78.7 Hz in bending (Fig. 5b) and the second at 112.4 Hz in torsion (Fig. 5c). The vibration modes at higher frequencies, which include the vibration of both cantilever and clamps, were not taken into account.

Two harmonic analyses were then performed to identify the system frequency response function (FRF) under either vertical or horizontal base acceleration. A harmonic acceleration with frequency from 10 to 200 Hz and 1g of amplitude was applied as enforced motion at the base.

The first harmonic analysis applied only a vertical base acceleration to have a bending loading at the notch. Figure 6a shows (solid line) the amplitude frequency response function (FRF) in terms of vertical acceleration of the specimen extremity (point B in Fig. 5a).

At low frequencies, the system response to bending loading is close to one and, when approaching the first resonance, it increases very rapidly. The same figure also reports, as a dashed line, the amplitude FRF in terms of horizontal acceleration of the cantilever beam extremity (point C in Fig. 5a). The dashed line starts from zero at low frequencies and presents two small peaks right on the first two resonances. These peaks can be explained by the constraint imposed by the thin plate: when the specimen bends and its extremity moves vertically, the thin plate also bends but not elongates, thus it induces a small rotation of specimen extremity and a corresponding horizontal displacement of point C.

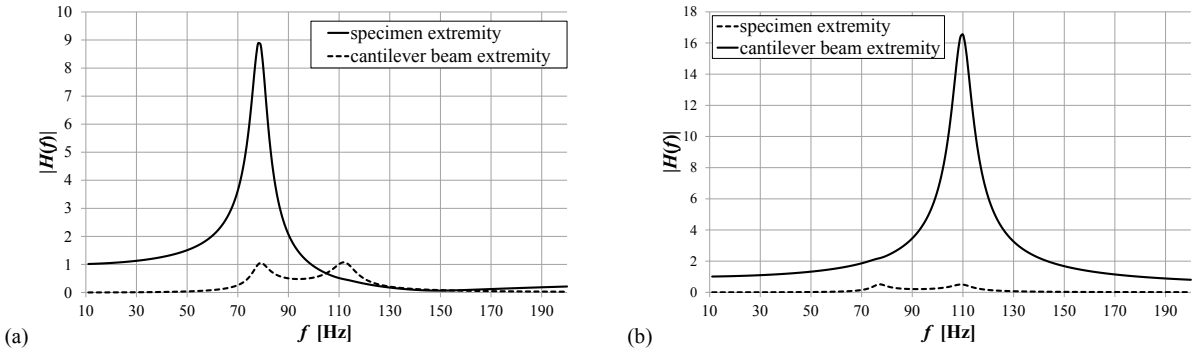

Fig. 6. Amplitude FRF $|H(f)|$ (a) under vertical acceleration and (b) under horizontal acceleration.

The second harmonic analysis applied only a horizontal base acceleration to have torsion loading at the notch. In Fig. 6b (solid line), the amplitude FRF in terms of horizontal acceleration of point C is shown. It has a trend similar to the graphs in Fig. 6a (but with a higher peak), although now the system response to torsion loading is amplified at the second resonance (112.4 Hz). The same figure also reports, as a dashed line, the amplitude FRF in terms of vertical acceleration of point B. Also in this case, the curve starts from zero at low frequencies and it presents two small peaks right on the first two resonances, which can be explained as described above.

The previous graphs point out that bending and torsion modes are weakly coupled, which makes not entirely true the hypothesis previously stated in Section 2. In fact, a fully uncoupled bending and torsion loading would require that the two dashed lines in Fig. 6 must be zero over all frequencies, and not only outside the two resonances. For this reason, the new system actually provides a fully uncoupled bending-torsion loading at least in the range of low frequencies, where the unavoidable contribution of the coupling term (dashed lines in Fig. 6) is almost zero.

After having investigated the system response under bending and torsional loading, it was necessary to choose the range of excitation frequency. The system can be excited in two different ways. The first is to excite at resonance, in which the stress response can be markedly amplified even with low input accelerations. In this case, two problems arise, yet: the response is always narrow-band and it is necessary to have a precise Input/Output control to remain at, or very close to resonance. The second way is to excite outside the resonance, for example at lower frequencies where the system FRF is flat and, therefore, a small variation of the excitation frequency does not cause a significant variation of response. Moreover, a flat FRF permits the system response to be similar to the input acceleration, for example also wide-band instead of being always narrow-band. Working outside resonance, however, requires greater acceleration amplitudes to have the specimen failure during the vibration tests.

In view of the above comments, it was agreed to excite the system outside the resonance. A reference excitation frequency of 20 Hz was chosen to verify whether the system is actually usable in tests. At this low frequency, in addition to have fully uncoupled bending and torsion (as showed in Fig. 6), the system also has a quasi-static behavior because the FRF is flat and close to one, so in first approximation the formula $F=m\cdot a$ is valid, as assumed in the analytical model.

Table 1. Input acceleration (in [g] unit) required by shaker tests: comparison between analytical and finite element model.

Loading type	Analytical model		Finite element model	
	[g] at $5\cdot10^4$ cycles	[g] at $2\cdot10^6$ cycles	[g] at $5\cdot10^4$ cycles	[g] at $2\cdot10^6$ cycles
Bending	6.502	5.475	8.666	7.296
Torsion	17.165	13.430	23.405	18.310

The FRF resulting from harmonic analysis was finally used to compute the input accelerations that give specimen failure at $5\cdot10^4$ and $2\cdot10^6$ cycles and to verify if the corresponding forces remain lower than the force limit F_{shaker} allowable by the tri-axis shaker. For example, a horizontal base acceleration of 23.405 g, required to have failure at $5\cdot10^4$ cycles under torsion, develops a force of 1.07 kN, see Table 1. The other accelerations (shown in Table 1) are even smaller, which then allows us to conclude that the new layout can be used for vibration tests with the available tri-axis shaker. Table 1 also compares the input accelerations required by the analytical model and the finite element model. It can be observed that the analytical model estimates smaller accelerations, the deviation being of the order of 25%. Nevertheless, these results confirm that the analytical model was a useful tool for a preliminary and fast estimate of input accelerations.

5. Experimental validation

Experimental validation is an essential phase to verify the results from numerical simulations and to prove that the system is really feasible for multi-axial fatigue tests. A Dongling tri-axis electrodynamic shaker (3ES-10-HF-500 model) was used to perform vibration tests (Fig. 7a). This brand new machine is capable of exciting simultaneously 3 orthogonal directions in the space, from 5 to 2000 Hz with a maximum rated force of 10 kN and a maximum rated velocity of 1.2 m/s. However, the shaker cannot excite only one single or two axes (channels). In any test, all three axes (channels) must always be activated simultaneously, which could be a problem if tests with two, or even only one acceleration, have to be performed. Nevertheless, this restriction can easily be overcome if the excitation level of the secondary channel/channels is set to a much lower level than the primary one. The controller and acquisition unit is a LMS SCADAS Mobile, driven by LMS Test.Lab software.

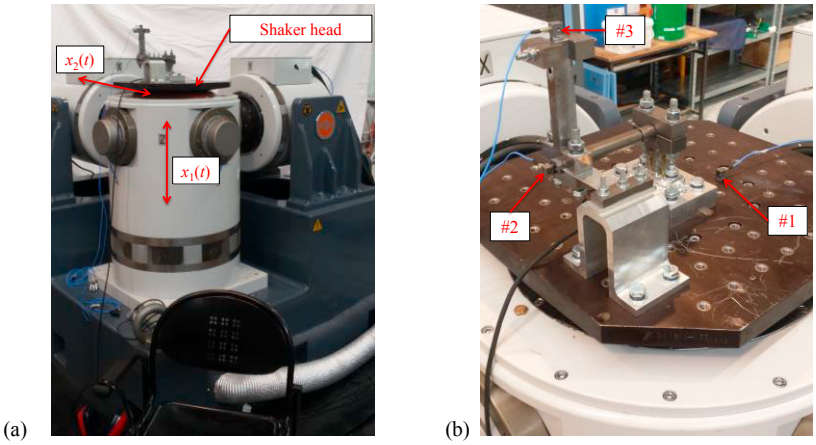

(a) (b)

Fig. 7. (a) Dongling tri-axis electrodynamic shaker; (b) testing system prototype mounted to the shaker head.

A prototype of the new system layout, described in Section 2, is mounted to the shaker head with screws and nuts, as shown in Fig. 7b. The measurement instruments used consist of a tri-axis accelerometer (#1) placed on shaker head to measure the input accelerations in closed loop control, and other two accelerometers (#2 and #3) for monitoring the system responses at the extremity of both the specimen and the cantilever beam.

As exhibited below, a harmonic analysis was performed in laboratory to measure the system response, with the aim to confirm if, at low frequencies, bending and torsion are fully uncoupled, as obtained in numerical simulations. Therefore, the tests were focused on a narrow frequency range (from 25 to 50 Hz) below the first resonance. Moreover, the influence of the phase shift (φ) between input accelerations was also investigated.

A first harmonic analysis applied, to the shaker head, two in-quadrature ($\varphi=\pi/2$) harmonic accelerations of 1g amplitude, with frequency varying from 25 to 50 Hz, in 1 Hz steps. The first acceleration $x_1(t)$ is along the vertical direction, the second $x_2(t)$ is along the horizontal direction perpendicular to the specimen axis (Fig. 7a). The other horizontal acceleration longitudinal to the specimen axis, not required to have bending and torsional loading, was significantly smaller and equal to 0.1g. A second similar harmonic analysis was also conducted by using in-phase ($\varphi=0°$) input accelerations.

The output accelerations were measured at the specimen extremity along the vertical direction (accelerometer #2 in Fig. 7b) and at the cantilever beam extremity along the horizontal direction (accelerometer #3).

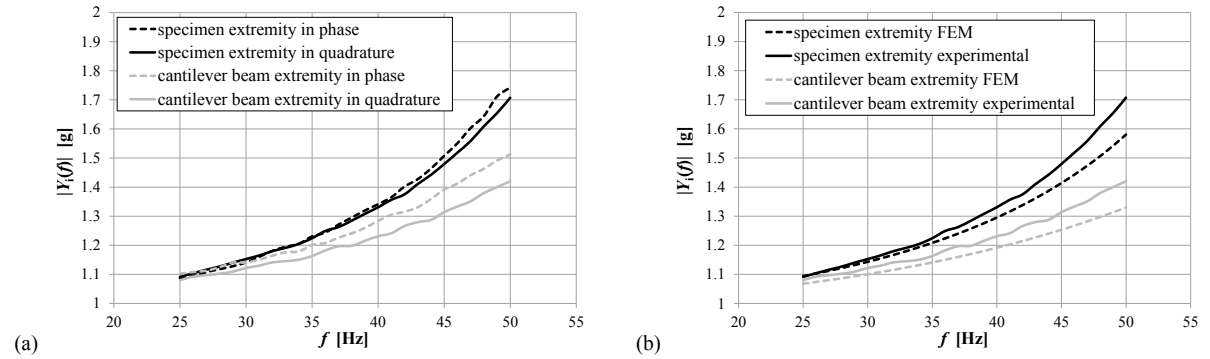

Fig. 8. (a) Output acceleration amplitudes $|Y_i(f)|$ with in-quadrature and in-phase input accelerations; (b) comparison between numerical and experimental output acceleration amplitudes $|Y_i(f)|$ for in-quadrature input accelerations.

Fig. 8a compares the acceleration amplitudes $|Y_i(f)|$ measured by accelerometers #2 and #3, for both in-quadrature and in-phase input accelerations. In both cases, a higher response amplitude results for in-phase input accelerations.

This trend can be explained by using the theory of Multi-Input/Multi-Output (MIMO) model, in which $x_1(t)$ and $x_2(t)$ are the input accelerations at the shaker head along vertical and horizontal directions, respectively, while $y_1(t)$ is the acceleration response at specimen extremity along vertical direction and $y_2(t)$ is the acceleration response at cantilever beam extremity along the horizontal direction (symbol t indicates time).

In matrix notation, the relationship in frequency domain between inputs and outputs is:

$$\{\mathbf{Y}(f)\} = \mathbf{H}(f)\{\mathbf{X}(f)\} \qquad \rightarrow \qquad \begin{Bmatrix} Y_1(f) \\ Y_2(f) \end{Bmatrix} = \begin{bmatrix} H_{11}(f) & H_{12}(f) \\ H_{21}(f) & H_{22}(f) \end{bmatrix} \cdot \begin{Bmatrix} X_1(f) \\ X_2(f) \end{Bmatrix} \tag{2}$$

where the column vectors $\{\mathbf{X}(f)\}$, $\{\mathbf{Y}(f)\}$ represent the Fourier Transform of $\mathbf{x}(t)=\{x_1(t), x_2(t)\}^T$, $\mathbf{y}(t)=\{y_1(t), y_2(t)\}^T$, while $[\mathbf{H}(f)]$ is the transfer function matrix, in which the term $H_{ij}(f)=Y_i/X_j$ represents the FRF when the system only has one input "j" and the response is measured at coordinate "i". By matrix product, each output response yields:

$$\begin{cases} Y_1(f) = X_1(f) \cdot H_{11}(f) + X_2(f) \cdot H_{12}(f) \\ Y_2(f) = X_2(f) \cdot H_{22}(f) + X_1(f) \cdot H_{21}(f) \end{cases} \tag{3}$$

Each output $Y_i(f)$ consists of two terms: the first one $H_{ii}(f)X_i(f)$ is the response for a Single-Input/Single-Output (SISO) model, while the second $H_{ij}(f)X_j(f)$ ($i \neq j$) is the response for an input in direction "i" and the output in direction "j" (if the out-of-diagonal terms $H_{ij}(f)$ were zero, the system would be fully uncoupled). The amplitude of $H_{ij}(f)$ (see the dashed lines in Fig. 6) are small but not exactly zero, therefore there is always a weak coupling between bending and torsion, as also discussed in Section 5.

It is now of interest to verify whether the coupling term depends on the relative phase φ between the two input acceleration signals $x_1(t)$ and $x_2(t)$. For a harmonic signal $x(t)=A\cdot\cos(2\pi f_0 t+\varphi)$ the Fourier Transform is $X(f)=(A/2)[e^{i\varphi}\delta(f+f_0)+e^{-i\varphi}\delta(f-f_0)]$, where $\delta(f-f_0)$ is the Dirac delta function (Gray and Goodman (1995)).

For a zero phase shift ($\varphi_1=\varphi_2=0$), both terms $X_1(f)$ and $X_2(f)$ are real functions of frequencies. Also the terms $H_{11}(f)$, $H_{22}(f)$, as well as the cross-terms $H_{12}(f)$, $H_{21}(f)$, are all real functions in the range of frequencies below resonance, which are considered in the present application (in that range, the system has a quasi-static response). As a result, all products $H_{ii}(f)X_i(f)$ and $H_{ij}(f)X_j(f)$ ($i \neq j$) are a real functions too. Therefore, the output responses $Y_1(f)$, $Y_2(f)$ are nothing but the sum of two real quantities and they are also in-phase with the input accelerations.

For a non-zero phase shift ($\varphi_1=0$, $\varphi_2=\pi/2$) between input accelerations $x_1(t)$ and $x_2(t)$, $X_1(f)$ still remains real, whereas $X_2(f)$ turns to an imaginary function of frequency. While the first product $H_{ii}(f)X_i(f)$ in Eq. (3) remains real, the second one $H_{ij}(f)X_j(f)$ becomes imaginary. As a result, the rule of parallelogram yields that the output responses $Y_1(f)$, $Y_2(f)$ are now lower than the in-phase case, and they are no longer in-phase with neither of the two input accelerations.

In summary, the sum between the two terms in Eq. (3) is maximized only if the two input accelerations are in-phase. This result is confirmed in Fig. 8a, which shows that the gap between in-phase and in-quadrature curves increases from 25 Hz to higher frequencies. This gap comes from the effect of φ on input accelerations.

Fig. 8b displays, instead, the comparison between numerical and experimental response amplitude acceleration for in-quadrature inputs ($\varphi_1=0$, $\varphi_2=\pi/2$). In the finite element analysis, two accelerations (vertical + horizontal) are now applied. The agreement between simulations and experiments can be considered to be reasonably good, by also considering that in the finite element model the contact surfaces were not modelled explicitly (e.g. bolted joints had perfectly glued surfaces). The experimental results then confirm the accuracy of the numerical model and that the designed system is feasible for multi-axial fatigue test on shaker. The experimental tests also proved the weak coupling between bending and torsion, which is however minimal or even negligible if the input accelerations are in-quadrature.

6. Conclusions

This research aimed to design a system allowing fully uncoupled bending and torsion loading in a vibration test on tri-axis shaker. Starting from the cantilever layout in Nguyen et al. (2011), in which bending and torsion are always coupled, the idea was to introduce a thin plate at the specimen free end to prevent bending when the specimen is loaded in torsion. Being very thin, this plate is flexible in bending and thus it should not impede the torsional rotation of the specimen.

Based on these considerations, an innovative testing layout was proposed. It is composed by a notched specimen and, at its extremity, by a cantilever beam with two tip masses. Both the specimen extremity and the cantilever beam are clamped to the base by the thin plate. To verify if the designed system was suitable to perform vibration tests on a tri-axis shaker available in the laboratory, several checks were carried out.

First, a lumped-mass model was developed to estimate the forces and input accelerations required to have specimen failure at $5\cdot10^4$ and at $2\cdot10^6$ cycles under bending and torsion loading, for a harmonic input acceleration. The results showed that the accelerations required in tests are perfectly compatible with shaker specifications.

A finite element model is then used to simulate the system dynamic behavior under horizontal and vertical accelerations and to calculate the required accelerations more accurately. The analysis of FRFs showed that a

horizontal excitation causes almost only a torsional loading induced by tip eccentric masses, while bending is fully impeded by the thin plate. Instead, a vertical excitation induces almost only a bending loading on the vertical plane. The numerical results thus confirmed that bending-torsion loading are fully uncoupled at least in the range of low frequencies (below resonance), whereas they are weakly coupled near the two resonances. Moreover, the input acceleration values necessary to specimen failure comply with the analytical ones, confirming the system expendability on our shaker.

Finally, experimental tests were performed to verify results of analytical model and numerical simulations. A system prototype was mounted to the shaker head and the response amplitudes were measured by accelerometers under harmonic input accelerations (from 25 Hz to 50 Hz) along vertical and horizontal directions. These experimental results showed a satisfactory agreement with numerical results and confirmed the presence of a weak coupling between bending and torsion loading (as also seen in numerical simulations), which is minimal or even negligible if input accelerations are in quadrature. The innovative system proposed in this work is then capable to produce fully uncoupled bending-torsion loading for vibrating tests in a tri-axis shaker. In the future, it will be exploited to perform vibration tests for investigating the fatigue life of specimens under bending-torsion stochastic loading.

Acknowledgements

This research was supported by the grant "*Fondo per l'Incentivazione alla Ricerca*" (FIR 2016) from the University of Ferrara.

References

Benasciutti, D., Tovo, R., 2005. Spectral Methods for Lifetime Prediction under Wide-band Stationary Random Processes. Int. Journal of Fatigue 27(8) 867–877.

Benasciutti, D., Tovo, R., 2006. Comparison of Spectral Methods for Fatigue Analysis of Broad-band Gaussian Random Processes. Probabilistic Eng. Mechanics 21(4) 287–299.

Benasciutti, D., 2014. Some Analytical Expressions to Measure the Accuracy of the "Equivalent von Mises Stress" in Vibration Multiaxial Fatigue. Journal of Sound and Vibration 333(18), 4326-4340..

Benasciutti, D., Sherratt, F., Cristofori, A., 2016. Recent Developments in Frequency Domain Multi-axial Fatigue Analysis. Int. Journal of Fatigue 91, 397–413.

Česnik, M., Slavić, J., Boltežar, M., 2012. Uninterrupted and Accelerated Vibrational Fatigue Testing with Simultaneous Monitoring of the Natural Frequency and Damping. Journal of Sound and Vibration 331(24), 5370–5382.

Ellyson, B., Brochu, M., Brochu, M., 2017. Characterization of Bending Vibration Fatigue of SLM Fabricated Ti-6Al-4V. Int. Journal of Fatigue 99, 25–34.

George, T., 2004. Development of a Novel Vibration-Based Fatigue Testing Methodology. Int. Journal of Fatigue 26(5), 477–486.

Ghielmetti, C., Ghelichi, R., Guagliano, M., Ripamonti, F., Vezzù, S., 2011. Development of a Fatigue Test Machine for High Frequency Applications. Procedia Engineering 10, 2892–2897.

Gray, R.M., Goodman J.W., 1995. Fourier Transforms. An Introduction for Engineers. Springer US.

Khalij, L., Gautrelet, C., Guillet, A., 2015. Fatigue Curves of a Low Carbon Steel Obtained from Vibration Experiments with an Electrodynamic Shaker. Materials and Design 86, 640–648.

Kim, C., Kang, Y., Lee, B., 2011. Experimental Spectral Damage Prediction of a Linear Elastic System Using Acceleration Response. Mechanical Systems and Signal Processing 25(7), 2538–2548.

Łagoda, T., Macha, E., Będkowski, W.X., 2000. Critical Plane Approach Based on Energy Concepts: Application to Biaxial Random Tension-Compression High-cycle Fatigue Regime. Int. Journal of Fatigue 21(5), 431–443.

Łagoda, T., Macha, Niesłony, A., 2005. Fatigue Life Calculation by Means of the Cycle Counting and Spectral Methods under Multiaxial Random Loading. Fatigue Fract. Eng. Mater. Struct. 28(4), 409–420.

Nguyen, N., Bacher-Höchst, M., Sonsino, C.M., 2011. A Frequency Domain Approach for Estimating Multiaxial Random Fatigue Life. Mat.-wiss. u. Werkstofftech. 42(10), 904–908.

Niesłony, A., Růžička, M., Papuga, J., Hodr, A., Balda, M., Svoboda, J., 2012. Fatigue Life Prediction for Broad-Band Multiaxial Loading with Various PSD Curve Shapes. Int. Journal of Fatigue 44, 74–88.

Pilkey, W., Pilkey, D., Peterson, R., 2008. Peterson's stress concentration factors. Hoboken, N.J.: John Wiley & Sons.

Schijve J., 2009. Fatigue of Structures and Materials. 2nd ed. Springer.

Zanellati, D., Benasciutti, D., Tovo, R., 2016. Studio dello Stato Tensionale di Vari Provini Intagliati per Prove Multiassiali a Flesso-torsione. 45° Congress of the Italian Association of Stress Analysis (AIAS), Trieste, 7-10 September 2016 (in Italian).